厚生労働科学研究費補助金（医療技術実用化総合研究事業）
分担研究報告書

陽子線高線量率ラインスキャニングの革新的技術の研究

前立腺癌に対する局所放射線治療に関する照射中の動きに関する臨床研究

研究分担者　白土　博樹　　北海道大学大学院医学研究科放射線医学分野
研究協力者　清水　伸一　　北海道大学大学院医学研究科放射線医学分野

研究要旨：陽子線高線量率ラインスキャンニング技術を利用するにあたり、前立腺癌での利用時に臨床的に従来のＸ線治療との比較をするための臨床試験のコンセプトを研究した。放射線治療中の前立腺の動き(intrafractional motion)は治療開始後 0-5 分、5-10 分以内では５-10 分のほうが大きかった。陽子線治療中には、intrafractional Motion に対する工夫をプロトコールに入れる必要が示された。

A．研究目的

動体追跡装置を用いて、前立腺癌治療中の前立腺の動き(Intra-fractional motion of the prostate)を減らすことが可能か否かを計測するための前向き検討試験。

B．研究方法

20 名の前立腺癌患者において、2ｍｍの金マーカーを前立腺近傍に 3 個刺入する。金マーカーの位置を7門強度変調放射線治療の門毎に把握し、2ｍｍ以上のずれがあれば、患者台を動かして、補正する。

C．研究結果

20 名の患者に関して 230 回の観察を行った。1 回の放射線治療において、平均 7.7 回の観察がなされた。放射線治療開始後 5 分間の動きは 99.5%のデータが、 -5.086 to 3.5 mm, -3.7 to 2.0 mm, and -1.4 to 2.4 mm であったが、５－１０分後は -7.20 to 6.74 mm、 -12.47 to 5.12 mm、-4.72 to 4.90 mm であり、時間経過とともに動きの範囲が広がることが示された。動体追跡装置を利用しているために、2ｍｍ以上の動きが観測された時点で、患者台の位置を是正することで、各患者の治療中の誤差を減らすことが可能であった。前立腺の動きには、□全く動きがないタイプ(Steady type)、□大きな動きのあるタイプ(large motion type)、□動きの増して行くタイプ（increasing motion type）の 3 種類があった。

D．　考察

動体追跡装置を利用して、腫瘍の動きを

門毎に観察することで、北海道大学病院では、2mm 以上の動きがあれば患者台を是正することで、治療中の動きは減らすことが可能であったが、同様の装置を持たない施設では、是正がなされていないはずである。 X線治療の場合には、ビームのずれは左右方向と頭尾方向には重要な意味を持つが、陽子線治療の場合にはさらに深さ方向のずれも大きな意味を持ち、数 mm のずれで distall falloff での線量低下が簡単に起きる、よって、陽子線治療では Intra-fractional motion を減らすことで、正確な放射線治療を実現することが可能であることが示唆された。

E. 結論

動体追跡装置を用いて、X線ＩMRTにおいて、ビーム毎に患者台の位置を補正することは、intra-fractional motion of the prostateによる誤差を減らすことが可能であった。陽子線治療では、治療中の前立腺位置のずれに対する配慮が必要である。

F. 研究発表

1. 論文発表

1) Park HC, Shimizu S, Yonesaka A, .. Shirato H. High dose three-dimensional conformal boost using the real-time tumor tracking radiotherapy system in cervical cancer patients unable to receive intracavitary brachytherapy. Yonsei Me J 2010; 51(1):93- 9.

2) Borst GR, Ishikawa M, Nijkamp J,..Shirato H, et al. Radiation Pneumonitis After Hypofractionated Radiotherapy: Evaluation of the LQ(L) Model and Different Dose Parameters. Int J Radiat Oncol Biol Phys. 2010 Mar 13. Epub ahead of print.

3) Bengua G, Ishikawa M, Sutherland K,..Shirato H. Evaluation of the effectiveness of the stereotactic body frame in reducing respiratory intrafractional organ motion using the real-time tumor-tracking radiotherapy system. Int J Radiat Oncol Biol Phys. 2010;77(2):630-6.

4) Homma A, Oridate N, Suzuki F,.. Shirato H, et al. Superselective high-dose cisplatin infusion with concomitant radiotherapy in patients with advanced cancer of the nasal cavity and paranasal sinuses: a single institution experience. Cancer. 2009 ;115(20):4705-14.

5) Nishioka K, Abo D, Aoyama H, .. Shirato H. Stereotactic radiotherapy for intracranial nonacoustic schwannomas including facial nerve schwannoma. Int J Radiat Oncol Biol Phys. 2009 ;75(5):1415-9

6) Borst GR, Ishikawa M, Nijkamp J, .. Shirato H, … et al. Radiation pneumonitis in patients treated for malignant pulmonary lesions with hypofractionated radiation therapy. Radiother Oncol. 2009 ;91(3):307-13

2. 学会発表

1) Onodera S, Aoyama H, Shirato H, et al. Fractionated Stereotactic Radiotherapy for Intracranial Meningioma: The Long-term Outcomes in Single Institution. Int J

Radiai Oncol Biol Phys 75(3), Sup 1. 2009: S256-S257.

G. 知的財産権の出願・登録状況（予定を含む）

1. 特許取得

なし

2. 実用新案登録

なし

3. その他

なし

厚生労働科学研究費補助金（医療技術実用化総合研究事業）
分担研究報告書

陽子線高線量率ラインスキャニングの革新的技術の研究

陽子線スキャニングビームの体内照射位置確認システムの研究

研究分担者　石川　正純　北海道大学大学院医学研究科先端医学講座

研究要旨：物理過程を推測するために必要な基本情報のうち、体内の元素分布をCT画像から取得し、体内元素分布とBOLPsによる陽電子放出核の放射能分布を同時に分析できるシステムの開発に着手し、体内を構成する元素の内、核反応に大きく寄与する核種として、水素、炭素、酸素、カルシウムについてCT画像から自動的にこれらの元素分布画像を表示できるシステムを作成した。

A．研究目的

国立がんセンター東病院に設置されている陽子線治療装置では、陽子線治療によって体内で核反応を起こす際に発生する陽電子放出核種を検出し、その放射能濃度分布を測定し、照射位置の検証や線量分布の評価を目的として Beam-on-line PET System (BOLPs)が設置されている。本研究では、陽子線スキャニングビームの体内照射位置確認システム開発の一環として、BOLPs によって得られたデータを解析するために、治療計画情報やCTデータなどと有機的な連携を持った解析システムを開発する。

B．研究方法

陽子線の照射により体内で核反応を起こして生成される陽電子放出核の生成過程には、多くの物理的現象が内在している。また、体内で核反応によって生成する陽電子放出核種は 1 種類ではなく、^{11}C, ^{13}N, ^{15}O, ^{18}F など複数存在し、それぞれの崩壊半減期も異なる。したがって、BOLPs で得られた 3 次元 PET 画像情報から、体内での核反応情報を推測するためには、様々な物理過程を推測できることが必要不可欠である。そこで、本分担研究では、その物理過程を推測するために必要な基本情報のうち、体内の元素分布をCT画像から取得し、体内元素分布とBOLPsによる陽電子放出核の放射能分布を同時に分析できるシステムの開発に着手した。

C．研究結果

体内元素分布の情報を直接調べることは困難であるため、Paganetti らによって報告された、体内を構成する組織に対する標準的な元素組成および密度を元に、CT値から体内の構成元素分布を推測する方法を参考にして、体内を構成する元素の内、核反応に大きく寄与する核種として、水素、炭素、酸素、カルシウムについてCT画像

から自動的にこれらの元素分布画像を表示できるシステムを作成した。

D． 考察

Paganetti の方法では、代表的な CT 値を元に構成元素情報を推測しているが、実際の生体では、組織内に含まれる水分量などによって、CT 値には若干の違いが生じる可能性がある。特に、血液は CT 値への影響が大きいため、毛細血管が発達している領域などでは、誤った元素として推測されてしまう可能性も考えられるので、CT 画像のみならず、MRI 画像などと有機的に連携し、血流情報を加味した元素予測なども考慮する必要がある。

E． 結論

物理過程を推測するために必要な基本情報のうち、体内の元素分布をCT画像から取得し、体内元素分布とBOLPsによる陽電子放出核の放射能分布を同時に分析できるシステムの開発に着手し、体内を構成する元素の内、核反応に大きく寄与する核種として、水素、炭素、酸素、カルシウムについてCT画像から自動的にこれらの元素分布画像を表示できるシステムを作成した。

F． 研究発表

1．論文発表

なし

2．学会発表

なし

G． 知的財産権の出願・登録状況（予定を含む）

1．特許取得

なし

2．実用新案登録

なし

3．その他

なし

研究成果の刊行に関する一覧表

雑誌

発表者氏名	論文タイトル名	発表誌名	巻号	ページ	出版年
T. Nishio, A. Miyatake, T. Ogino, K, Nakagawa, N. Saijo, H. Esumi	The development and clinical use of a beam ON-LINE PET system mounted on a rotating gantry port in proton therapy	Int. J. Radiat. Oncol. Biol. Phys.	76(1)	277-286	2010
R. Kohno, E. Hirano, S. Kitou, T. Goka, K. Matsubara, S. Kameoka, T. Matsuura, T. Ariji, T. Nishio, M. Kawashima, T. Ogino	Evaluation of the usefulness of a MOSFET detector in an anthropomorphic phantom for 6-MV photon beam	Radiol. Phys. Technol.	In press		2010
Park HC, Shimizu S, Yonesaka A, .. Shirato H.	High dose three-dimensional conformal boost using the real-time tumor tracking radiotherapy system in cervical cancer patients unable to receive intracavitary brachytherapy	Yonsei Me. J.	51(1)	93- 9	2010
Borst GR, Ishikawa M, Nijkamp J,..Shirato H, et al.	Radiation Pneumonitis After Hypofractionated Radiotherapy: Evaluation of the LQ(L) Model and Different Dose Parameters	Int. J. Radiat. Oncol. Biol. Phys.	Epub ahead of print		2010
Y. Egashira, T. Nishio, S. Kameoka, T. Matsuura, M. Uesaka	Initial evaluation of delta-functional multi segmented pencil beam algorithm for proton therapy	Abstract book, PTCOG 49		207	2010
T. Nishio, A. Miyatake, T. Tachikawa, M. Yamada, T. Ogino	The clinical use of the beam ON-LINE PET system mounted on a rotating gantry port in proton therapy	Abstract book, PTCOG 49		177	2010

Y. Takada, K. Hotta, R. Kohno, T. Himukai, Y. Hara, T. Nishio	Improvement of beam-use efficiency for double-scattering method using a multiple-ring second scatterer in proton therapy	Abstract book, PTCOG 49		171	2010
J. Inoue, M. Tachibana, T. Ochi, T. Morita, T. Tachikawa, T. Asaba, M. Hirabayashi, Y. Kumata, T. Nishio, T. Ogino	Development of beam position monitoring system for pencil beam scanning	Abstract book, PTCOG 49		169	2010
T. Tachikawa, Y. Arai, T. Ochi, T. Nishio, T. Ogino	Fine-pitch multi-leaf collimator for proton therapy system	Abstract book, PTCOG 49		168	2010
R. Kohno, K. Hotta, K. Matsubara, T. Matsuura, S. Kameoka, T. Nishio, M. Kawashima, T. Ogino	In-vivo dosimetry using a MOSFET detector in an anthropomorphic phantom for therapeutic proton beam	Abstract book, PTCOG 49		129	2010
T. Matsuura, Y. Egashira, T. Nishio, Y. Matsumoto, Y. Furusawa, M. Wada, S. Koike, Y. Kase, T. Ogino	The biological effect of high-dose-rate proton beam on HSG cell	Abstract book, PTCOG 49		78	2010
M. Wada, Y. Matsumoto, T. Matsuura, Y. Egashira, S. Koike, A. Kanemoto, T. Nishio, N. Matsufuji, Y. Furusawa	Enhanced radiobiological effects at distal-end of proton SOBP beam	Abstract book, PTCOG 49		51	2010
T. Asaba, T. Tachikawa, M. Yamada, T. Ochi, J. Inoue, T. Nishio, T. Ogino	3D irradiation of pencil beam scanning	Abstract book, PTCOG 49		45	2010

T. Nishio	Proton Therapy	Jpn. J. Med. Phys. Proc.	30 Supple. 1	59-68	2010
R. Kohno, K. Hotta, K. Matsubara, T. Matsuura, S. Kameoka, T. Nishio, M. Kawashima, T. Ogino	A new correction method of a MOSFET response for in-vivo dosimetry in proton beam therapy	Jpn. J. Med. Phys. Proc.	30 Supple. 2	336-337	2010
T. Matsuura, Y. Egashira, T. Nishio, K. Matumoto, M. Wada, Y. Furusawa, S. Koike, K. Matsumura, T. Ohta, H. Suzuki, T. Toda, T. Taniyama, T. Shimojyu, A. Sakamoto, S. Minakami, M. Kawashima, T. Ogino	Proton high dose rate effect on HSG cell survival curve	Jpn. J. Med. Phys. Proc.	30 Supple. 2	239-240	2010
T. Nishio, A. Miyatake, K. Nakagawa, T. Ogino, N. Saijo, H. Esumi	Study of Molecular Image Guided Intensity Modulated Proton Therapy	Jpn. J. Med. Phys. Proc.	30 Supple. 2	233-234	2010
Y. Sugama, T. Nishio, K. Maruyama	A comparison of dose distributions of IMPT and IMRT with the treatment-planning system XiO	Jpn. J. Med. Phys. Proc.	30 Supple. 2	119-120	2010
S. Tomori, Y. Sugama, S. Akita, H. Seto, H. Takei, T. Nishio, T. Kawabata, K. Maruyama	Examination of the evaluation method of beam broadening by transforming inhomogeneous matter into water equivalent thickness for proton beam therapy	Jpn. J. Med. Phys. Proc.	30 Supple. 2	117-118	2010

T. Nishio, S. Tomori, K. Maruyama, T. Ogino	Development of an easy-to-handle measurement tool of pencil beam dose distribution for proton scanning irradiation	Jpn. J. Med. Phys. Proc.	30 Supple. 2	115-116	2010
Y. Egashira, T. Nishio, K. Matumoto, T. Matsuura, M. Uesaka	Initial verification of Delta-functional Multi Segmented Pencil Beam Algorithm for proton therapy	Jpn. J. Med. Phys. Proc.	30 Supple. 2	111-112	2010
西尾禎治	高精度放射線治療実施先行施設：国立がんセンター東病院における頭頸部IMRT	第２１回の日本高精度放射線外部照射研究会シンポジウム−高精度放射線治療広域展開時代を迎えて〜先行施設と新規開始施設の対話抄録集		26	2010
西尾禎治	PETを利用した高精度陽子線治療技術の展望	ISOTOPE NEWS	667	8-16	2009
H. Tujii, T. Akagi, K. Akahane, Y. Uwamizo, T. Ono, T. Kanai, R. Kohno, T. Sakae, M. Shimizu, E. Urakabe, T. Nakayama, T. Nakamura, T. Nishio, K. Nishizawa, S. Fukuda, N. Matsufuji, H. Yamashita, S. Yonai,	Research on Radiation Protection in the Application of New Technologies for Proton and Heavy Ion Radiotherapy	Jpn. J. Med. Phys.	28(4)	172-206	2009
T. Nishio, S. Kameoka	Utilization of Monte Carlo Simulation Toolkit GEANT4 for Proton Therapy	J. J. Simu. Technol.	28(1)	34-40	2009

Nakajima T, Nihei K, et al.	A phase I trial of 5-fluorouracil with cisplatin and concurrent standard-dose radiotherapy in Japanese patients with stage II/III esophageal cancer	Jpn. J. Clin. Oncol.	39(1)	37-42	2009
Onozawa M, Nihei K, et al.	Elective nodal irradiation (ENI) in definitive chemoradiotherapy (CRT) for squamous cell carcinoma of the thoracic esophagus	Radiother. Oncol.	92(2)	266-269	2009
Homma A, Oridate N, Suzuki F,.. Shirato H, et al.	Superselective high-dose cisplatin infusion with concomitant radiotherapy in patients with advanced cancer of the nasal cavity and paranasal sinuses: a single institution experience	Cancer	115(20)	4705-14	2009
Nishioka K, Abo D, Aoyama H, .. Shirato H.	Stereotactic radiotherapy for intracranial nonacoustic schwannomas including facial nerve schwannoma	Int. J. Radiat. Oncol. Biol. Phys.	75(5)	1415-9	2009
Borst GR, Ishikawa M, Nijkamp J, .. Shirato H, ... et al.	Radiation pneumonitis in patients treated for malignant pulmonary lesions with hypofractionated radiation therapy	Radiother. Oncol.	91(3)	307-13	2009
T. Nishio, A. Miyatake, T. Tachikawa, M. Yamada	The beam ON-LINE PET system mounted on a rotating gantry port for proton therapy in National Cancer Center. Kashiwa	Abstract book, PTCOG 48		27	2009

K. Hotta, R. Kohno, Y. Takada, R. Tansho, Y. Hara, T. Himukai, S. Kameoka, T. Nishio	Verification of simplified Monte Carlo algorithm in treatment planning for proton cancer therapy	Abstract book, PTCOG 48		45	2009
T. Asaba, T. Tachikawa, T. Ochi, M. Yamada, T. Nishio, T. Ogino	Development of pencil beam scanning nozzle system	Abstract book, PTCOG 48		84	2009
T. Tachikawa, T. Ochi, T. Asaba, M. Yamada, T. Nishio, T. Ogino	Multi-purpose nozzle for pencil beam scanning and wobbling	Abstract book, PTCOG 48		85	2009
R. Kohno, K. Hotta, S. Kameoka, T. Matsuura, T. Nishio, M. Kawashima, T. Ogino	Measurements of dose distribution using a MOSFET detector for therapeutic proton beam	Abstract book, PTCOG 48		101	2009
A. Miyatake, T. Nishio, T. Tachikawa, M. Yamada	Simulation system of positron emitter nuclei distribution in a patient body using target elemental activity pencil beam algorithm in proton therapy	Abstract book, PTCOG 48		122-123	2009
K. Hotta, R. Kohno, Y. Takada, Y. Hara, R. Tansyo, T. Himukai, T. Nishio	Verification of simplified Monte Carlo algorithm for clinical use in proton radiotherapy treatment planning	Jpn. J. Med. Phys. Proc.	29 Supple. 3	35-36	2009
M. Kaburagi, T. Matsuura, S. Kameoka, T. Nishio, M. Uesaka	The utility of Monte Carlo simulation GEANT4 in proton therapy	Jpn. J. Med. Phys. Proc.	29 Supple. 3	50-51	2009

R. Kohno, K. Hotta, S. Kameoka, K. Matsubara, T. Matsuura, T. Nishio, M. Kawashima, T. Ogino	Measurements of dose distributions using a MOSFET detector for therapeutic proton beams	Jpn. J. Med. Phys. Proc.	29 Supple. 3	54-55	2009
西尾禎治、宮武彩	原子核反応を利用した画像誘導高精度陽子線治療	高LET放射線研究会～物理・化学・生物の基礎研究から医学応用まで～	HIMAC-133	1-2	2009
西尾禎治、宮武彩、亀岡覚	電子線治療における高磁場を利用した患者体内中線量分布制御法	第２０回日本高精度放射線外部照射研究会、抄録集		61	2009
西尾禎治、宮武彩、中川恵一、荻野尚、西條長宏、江角浩安	患者体内中における原子核破砕反応を利用した画像誘導陽子線治療法	第２０回日本高精度放射線外部照射研究会、抄録集		43	2009
西尾禎治	粒子線治療における物理的有用性	第４８回日本医学放射線学会生物部会学術大会　第３９回放射線による制癌シンポジウム−基礎と臨床の対話−日講演要旨集		54-55	2009

書籍

著者氏名	論文タイトル名	書籍全体の編集者名	書　籍　名	出版社名	出版地	出版年	ページ
西尾禎治	医療機関における医学物理の重要性		治療学７：放射線治療（根治から症状緩和まで）	ライフサイエンス出版	東京	2009	19-23

研究成果の刊行物・別刷

ELSEVIER

Int. J. Radiation Oncology Biol. Phys., Vol. 76, No. 1, pp. 277–286, 2010

0360-3016/10/$–see front matter

doi:10.1016/j.ijrobp.2009.05.065

PHYSICS CONTRIBUTION

THE DEVELOPMENT AND CLINICAL USE OF A BEAM ON-LINE PET SYSTEM MOUNTED ON A ROTATING GANTRY PORT IN PROTON THERAPY

TEIJI NISHIO, PH.D.,*† AYA MIYATAKE, M.SC.,‡ TAKASHI OGINO, M.D.,* KEIICHI NAKAGAWA, M.D.,† NAGAHIRO SAIJO, M.D.,§ AND HIROYASU ESUMI, M.D.||

From the *Particle Therapy Division, Research Center for Innovative Oncology, National Cancer Center, Kashiwa; †Department of Radiology, Graduate School of Medicine, University of Tokyo; ‡Department of Nuclear Engineering and Management, Graduate School of Engineering, University of Tokyo; §Deputy Director, National Cancer Center, Kashiwa; and ||Director, National Cancer Center, Kashiwa

Purpose: To verify the usefulness of our developed beam ON-LINE positron emission tomography (PET) system mounted on a rotating gantry port (BOLPs-RGp) for dose–volume delivery-guided proton therapy (DGPT).
Methods and Materials: In the proton treatment room at our facility, a BOLPs-RGp was constructed so that a planar PET apparatus could be mounted with its field of view covering the iso-center of the beam irradiation system. Activity measurements were performed in 48 patients with tumors of the head and neck, liver, lungs, prostate, and brain. The position and intensity of the activity were measured using the BOLPs-RGp during the 200 s immediately after the proton irradiation.
Results: The daily measured activity images acquired by the BOLPs-RGp showed the proton irradiation volume in each patient. Changes in the proton-irradiated volume were indicated by differences between a reference activity image (taken at the first treatment) and the daily activity-images. In the case of head-and-neck treatment, the activity distribution changed in the areas where partial tumor reduction was observed. In the case of liver treatment, it was observed that the washout effect in necrotic tumor cells was slower than in non-necrotic tumor cells.
Conclusions: The BOLPs-RGp was developed for the DGPT. The accuracy of proton treatment was evaluated by measuring changes of daily measured activity. Information about the positron-emitting nuclei generated during proton irradiation can be used as a basis for ensuring the high accuracy of irradiation in proton treatment. © 2010 Elsevier Inc.

Dose–volume delivery guided proton therapy (DGPT), Beam ON-LINE PET system on rotating gantry port (BOLPs-RGp), Target nuclear fragment reaction.

INTRODUCTION

Proton therapy is a form of radiotherapy that enables the concentration of a dose onto a tumor by the use of a scanned or modulated Bragg peak. Therefore, it is very important to evaluate the proton-irradiated volume accurately.

Recently, to ensure the high accuracy of proton therapy, imaging studies of positron-emitting nuclei that are generated by target nuclear fragment reactions involving incident protons and nuclei from a patient's body have been performed (1–14). The annihilation gamma rays from the positron-emitting nuclei were measured by a positron emission tomography (PET) system (specifically a beam OFF-LINE PET system using commercial PET apparatus or PET-computed tomography [CT] apparatus postirradiation or a beam ON-LINE PET system in a proton treatment room). The beam OFF-LINE PET system using the commercial PET-CT apparatus has the advantage of being able to easily acquire fusion images and the ability to reconstruct three-dimensional images. However, the time required for the movement of the patient to the PET room (10–30 min) and the resulting deterioration of the statistical accuracy of the acquired data are large disadvantages. With the beam ON-LINE PET system, capturing a large view and the acquisition of three-dimensional images are difficult because of geometrical problems caused by the beam direction and the PET apparatus (7, 15, 16).

Reprint requests to: Teiji Nishio, Ph.D., Particle Therapy Division, Research Center for Innovative Oncology, National Cancer Center, Kashiwa 6-5-1 Kashiwano-ha, Kashiwa-shi, Chiba 277-8577, Japan. Tel: (+81) 4-7133-1111; Fax: (+81) 4-7134-7048; E-mail: tnishio@east.ncc.go.jp

Conflict of interest: none.

Supported by Health and Labour Science Research Grants from the Japanese Government.

Acknowledgment—The authors would like to thank the staff members of the Proton Radiotherapy Department of the National Cancer Center, Kashiwa for their help and the members of SHI Accelerator Service, Ltd., and Accelerator Engineering, Inc., for operating of the proton apparatus. We also acknowledge T. Okamoto of Hamamatsu Photonics, K. K., T. Tachikawa of Sumitomo Heavy Industries, Ltd., and H. Oka of SGI Japan, Ltd., for their technical support.

Received Jan 6, 2009, and in revised form May 28, 2009. Accepted for publication May 29, 2009.

The ability to take daily PET images with a high statistical accuracy while the patient remains in the proton irradiation room is a large advantage. Besides, availability of a cone beam (CB) CT system or CT apparatus in the irradiation room can offer the possibility of daily and in situ monitoring of the patient's anatomy. A prototype beam ON-LINE PET system (BOLPs) was previously constructed for basic research (10), and verification of the proton-irradiated volume in a patient's body was confirmed using a PET apparatus and a PET-CT apparatus (beam OFF-LINE PET system) (13).

A BOLPs mounted on a rotating gantry port (BOLPs-RGp) was constructed in our proton treatment room. Activity measurement and PET imaging were performed in 48 patients with tumors of the head and neck, liver, lungs, prostate, and brain during proton treatment at our facility. The position and intensity of the activity were measured daily using the BOLPs-RGp immediately after proton irradiation. Using the activity measurement, we were able to confirm whether the proton beam irradiation of the tumor was reproducibly performed during the treatment period. Moreover, changes in the activity distribution were observed as the volume of the tumor changed, and these changes were related to the delivery dose, changes in the body shape and position of the patient, and the physiologic changes. The PET images from the BOLPs-RGp were sufficient to provide high-quality proton treatment.

METHODS AND MATERIALS

Design of a beam ON-LINE PET system mounted on an RGp

Via the detection of pairs of annihilation gamma rays emitted from the generated radioactive nuclei of a patient's body, the BOLPs-RGp is designed to determine the position and activity of the positron-emitting nuclei generated in patients by proton irradiation. Figure 1 is a picture of the BOLPs-RGp. The BOLPs-RGp was developed as a standardized system for use with proton therapy devices. During proton therapy, the detector heads have many degrees of freedom and the system allows remote control adaptation to each new proton beam condition and a patient's position. As a result, the measurement of the activity distribution is simple.

A planar positron imaging system (Hamamatsu Photonics K. K., Hamamatsu, Japan) (17) was newly arranged for the BOLPs-RGp. In comparison to the system used previously (10), the 24 detector units mounted on each detector head were increased to 36 detector units, and each unit was composed of 11 × 10 arrays of BGO ($Bi_4Ge_3O_{12}$) crystals with a crystal size of 2 × 2 × 20 mm^3. Furthermore, the 2,400 crystals were increased to 3,600 crystals. The gap of each unit became 3.3 mm from 11.0 mm for minimizing dead space in the detector. The field of view (FOV) became 164.8 × 167.0 mm^2 from 120.8 × 186.8 mm^2. The maximum field size is 185.0 × 185.0 mm^2 in the rotating gantry port with the BOLPs-RGp. Therefore, the FOV can almost cover each treatment site of the head and neck, liver, lungs, prostate, and brain for a proton treatment in our facility. However, in case of prostate, the depth activity distribution is not measured in the entranee of the incident proton beam. The BOLPs-RGp was mounted on and the center of its detection area was aligned with the iso-center of the rotating gantry in the treatment room of the proton therapy facility at our center. A PET image reconstructed by a back-projection method

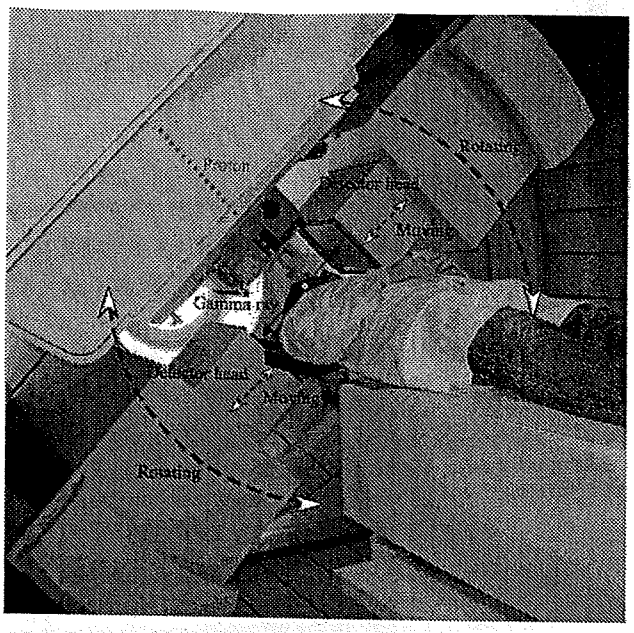

Fig. 1. Setup of the BOLPs-RGp, which is mounted on the rotating gantry port of our proton treatment room.

along the axis of the proton beam direction is always included in the FOV of the opposing detectors together with the axis of the rotating angle of the gantry system. The distance between the two opposing detector heads of the BOLPs-RGp can be adjusted from 30 to 100 cm. When the activity is not being measured, the detector head is stored inside the wall of the gantry device. The position resolution of this system is about 2 mm for the full width at half maximum in the case of use of ^{22}Na point source. The maximum data collection rate for the coincident detection of pair annihilation gamma rays is about 4,000 counts/s/cm^2 (kcps/cm^2). The accuracy of the measurements of activity distribution by this system was verified by a prototype beam ON-LINE PET system (10). The measured data are stored using in the software's list mode format. The activity image is renewed every second. The information of the on-off time points of beam irradiation is recorded in the data, and the image can be restructured according to this information. The PET data from the irradiation field of each patient are managed throughout each treatment day.

The detection efficiency of the distance between the detector heads was calibrated by using the thin-flat acrylic container filled with ^{18}F-solution. The calibration is used for a correction of the imaging uniformity and the detection sensitivity. The attenuation coefficient of 511-keV gamma rays in the patient's body was calculated by the patient's CT image data. They are used for a construction of the activity imaging. The correction of the photon scattering in the patient's body is not considered for the activity imaging. Furthermore, the photons scattered in the patient's body outside the FOV are detected by the effect of the geometry of the detector head. Therefore, the activity image is contaminated by about 10% background in this system. As the result, the position resolution of the activity distribution will become large more than 2 mm in the clinical case of a proton therapy.

Activity measurement in a patient during proton treatment

The measurement of activity was performed daily in 48 cases involving tumors of the head and neck, liver, lungs, prostate, and brain

using the BOLPs-RGp. The position and intensity of activity were measured during the 200 s immediately after proton irradiation using the trigger signal of the beam-off time. The measurement was performed using the shortest possible distance between the two opposing detector heads of the BOLPs-RGp for each patient. The average distance of the detector heads was 40 cm for the head and neck and the brain, 70 cm for the liver and the lungs, and 50 cm for the prostate. The time of 200 s after proton beam irradiation was chosen according to the intensity of activity estimated from the results of other studies (10, 13). The activity data obtained during proton irradiation were not used for PET imaging. Various types of background radiation (X-rays, gamma rays, and neutrons) occur during proton beam irradiation, and the quality of the activity image becomes markedly worse in their presence (2, 10, 15, 16). Furthermore, high radiation decreases the accuracy of the detector.

Verification of activity measurement was performed in 18, 4, 15, 10, and 1 cases involving tumors of the head and neck, the liver, the lungs, the prostate, and the brain, respectively. The typical fractional dose is 2.5 Gy equivalents (GyE = Gy × the relative biologic effectiveness: [= 1.1 = constant]) for the head and neck, 3.8 GyE for the liver, 4.0 GyE for the lungs, 2.0 GyE for the prostate, and 2.5 GyE for the brain in our facility. The irradiated field is typically planned with three fields in the head and neck and two fields in other sites. Furthermore, the typical number of irradiated field per fractional dose is one in the head and neck, liver, and prostate, and two in the lungs. The fractional dose was delivered over an irradiation time of 10–300 s. The proton beam irradiation was synchronized with the organ motion caused by respiration in the liver and the lungs.

Procedure for clinical use of activity image

A flow chart of procedure for clinical use of the BOLPs-RGp is shown in Fig. 2. In the clinical use, the main operation is to take an activity image every day and compare the activity image of the first day of treatment with each activity image during the comparatively long period of the treatment. If the difference of both the images is confirmed by reducing of the tumor size and changing of the body shape, then the new dose distribution is obtained from redose calculation of the plan on a new CT image acquisition, and the first proton treatment plan is immediately corrected to the new plan. As a result, proton treatments of high accuracy can be offered to the patient by keeping of the planned dose delivery.

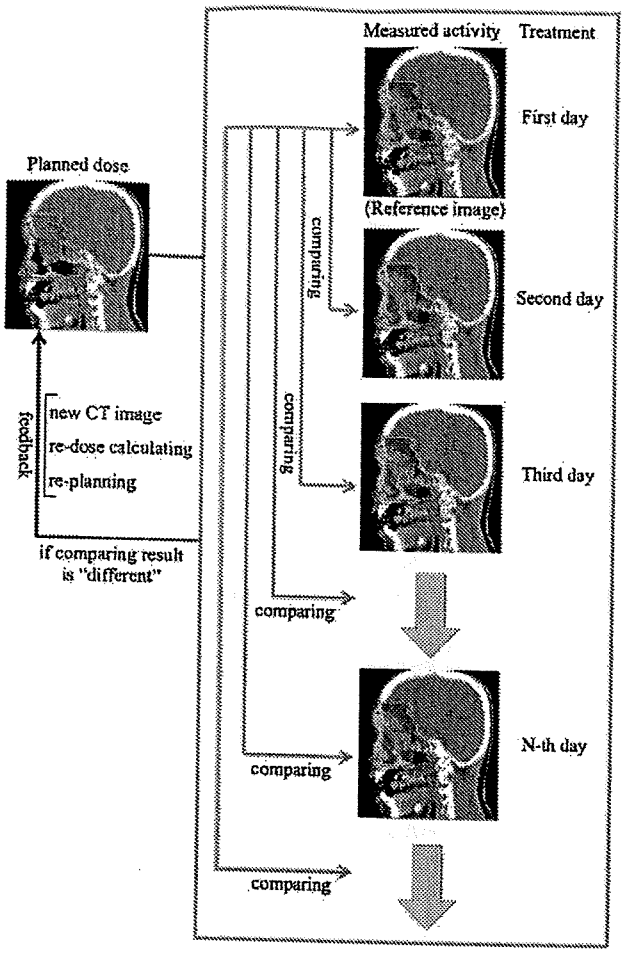

Fig. 2. Flow diagram of the procedure for the clinical use of the BOLPs-RGp.

RESULTS

Estimation of the measurement time for PET imaging

An estimation of an appropriate measurement time for PET imaging was performed using the measured activity data from tumors of the head and neck. The proton beam conditions were as follows: an energy of 120 MeV, a spread out of Bragg peak (SOBP) of 80-mm width, a gantry angle of 340°, a fractional dose of 2.5 GyE, and an irradiation time of 24 s. The distance between the detector heads was 70 cm, and the detection rate of the activity was 1.5 kcps. The left panel of Fig. 3 shows the number of detection events per volume during the detection period after proton beam irradiation. The statistical error (= standard deviation/mean value) decreased as the detection time increased. The error was 2.8% for a 200-s detection time, 3.0% for 150 s, 3.4% for 100 s, and 4.4% for 50 s. The right panel of Fig. 3 shows PET images taken using detection times of (a) 0, (b) 50, (c) 100, and (d) 200 s.

PET images of each treatment site

Typical PET images obtained by the BOLPs-RGp are shown for each case involving tumors of the head and neck, the liver, the lungs, the prostate, and the brain. Figure 4 shows the calculated dose distribution and the measured activity distribution on the first treatment day. The beam irradiation parameters were shown in Table 1. The PET images were obtained during the 200 s after proton beam irradiation. The mean detection rates of the activity generated in the proton beam irradiated volume were 1.58, 1.39, 0.53, 1.08, and 1.85 kcps, respectively. The color line and wash normalized to the iso-center show the dose distribution and activity distribution, respectively. By comparing and verifying between the calculated dose distribution and the measured activity distribution, it can be confirmed visually and roughly that the proton beam has irradiated the tumor. In cases of the liver and the lungs, the length of beam irradiation time is adjusted according to the stability of respiration on the treatment day and the patient. By the effect of organ motion, the number of

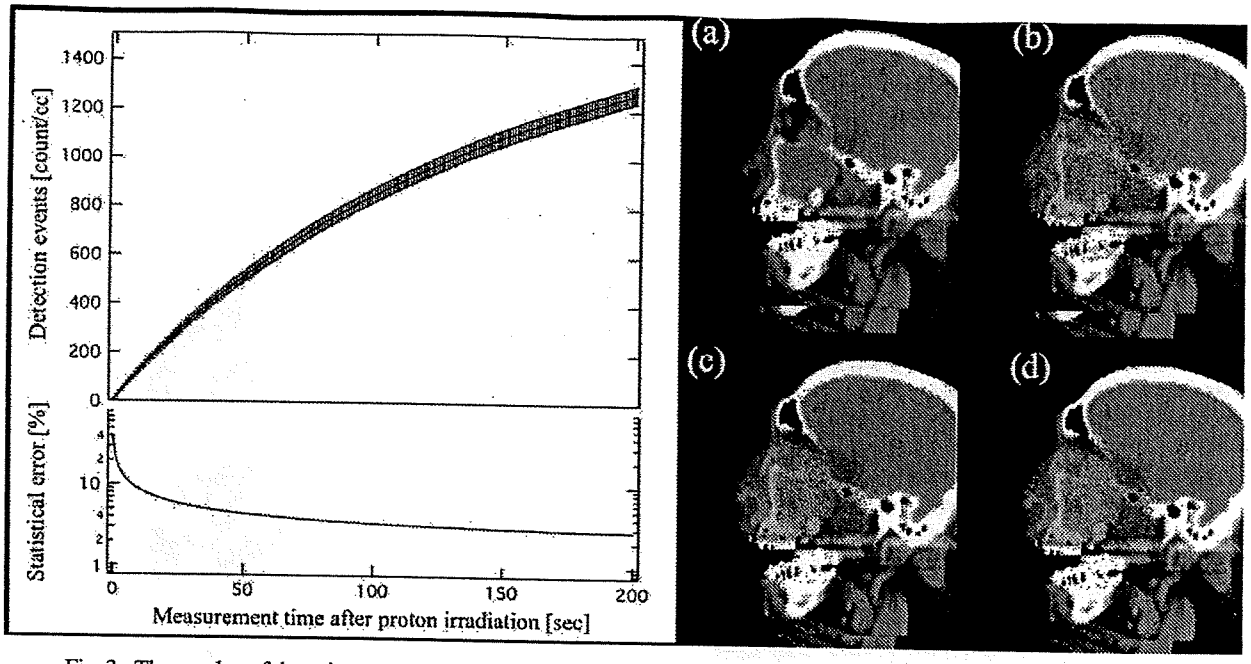

Fig. 3. The number of detection events per volume and PET images obtained during the detection period after proton beam irradiation. The PET images for detection period of (a) 0, (b) 50, (c) 100, and (d) 200 s are shown.

the detection event of the activity measured in the gating window will became about one third of the total detection events, and the statistical error will increase. Therefore, the measurement was performed with no synchronization with organ motion by respiration.

Changes in the activity distribution during the treatment period

In each treatment site, the activity distribution changed probably by reduction of the tumor size and changing of the body shape was conspicuously observed in some cases of the head and neck.

The verification was performed for a case involving tumors of the head and neck. Proton beam irradiation was performed in three fields of view: Port 1: 123 MeV, 90-mm SOBP, 350° gantry angle, 0° bed angle; Port 2: 121 MeV, 90-mm SOBP, 10° gantry angle, 20° bed angle; and Port 3: 117 MeV, 80-mm SOBP, 340° gantry angle, 350° bed angle. The irradiation dose was 2.5 GyE. Figure 5 shows a calculated proton dose distribution, an activity distribution, and a depth profile of a 2.5-GyE dose irradiation after a delivery dose of 2.5 (reference image), 10.0, 17.5, or 32.5 GyE from Port 1, a delivery dose of 5.0 (reference image), 12.5, 20.0, or 35.0 GyE, from Port 2, and a delivery dose of 7.5 (reference image), 15.0, 22.5, or 30.0 GyE from Port 3. Changes of the activity distribution were observed according to changes of the proton beam range and the dose delivered by previous irradiations resulted in a reduction of the tumor (see the arrow and the area surrounded by the dotted line in Fig. 5). The changing values of the activity range for each irradiation field (Port 1, Port 2, and Port 3) are shown in upper left of Fig. 6.

The activity range was defined by the depth point of 50% distal falloff in the activity distribution normalized at the iso-center. The changing value of the activity range fully exceeded a 10-mm length. Moreover, to observe the changes in the activity distribution in the depth direction in a similar manner, the ratio of the integration of the detected numbers between 20 mm and 70 mm from the iso-center was expressed as follows:

$$R(D) = \frac{\int_{20}^{70} \left(dA(D)/dZ\right) dz}{\int_{20}^{70} \left(dA(0)/dZ\right) dz}. \quad (1)$$

Here, z is the depth, D is the delivery dose, A(D) is the depth activity distribution, and A(0) is the reference depth activity distribution. The ratio of the delivery dose is shown in the middle left of Fig. 6. The bottom left of Fig. 6 is the proton beam irradiation time per fraction dose at each irradiation. The average of the irradiation time was 30 s, and the difference of the irradiation time at random was within 3 s.

In this case, a new CT image was scanned and a retreatment planning was produced after the delivery of 35 GyE of the prescribed dose of 65 GyE. The volume of the tumor was decreased from 184 mL to 125 mL (the arrow in right of Fig. 6 shows the visible tumor reduction), and the maximum beam range was shortened by 20-mm water equivalent length. In the other 2 cases of 18 clinical cases of the head and neck, the changing activity range of more than 10 mm was observed. Similarly, the new CT image acquisition and the retreatment planning were immediately performed after the observation of the changing activity range. The reduction

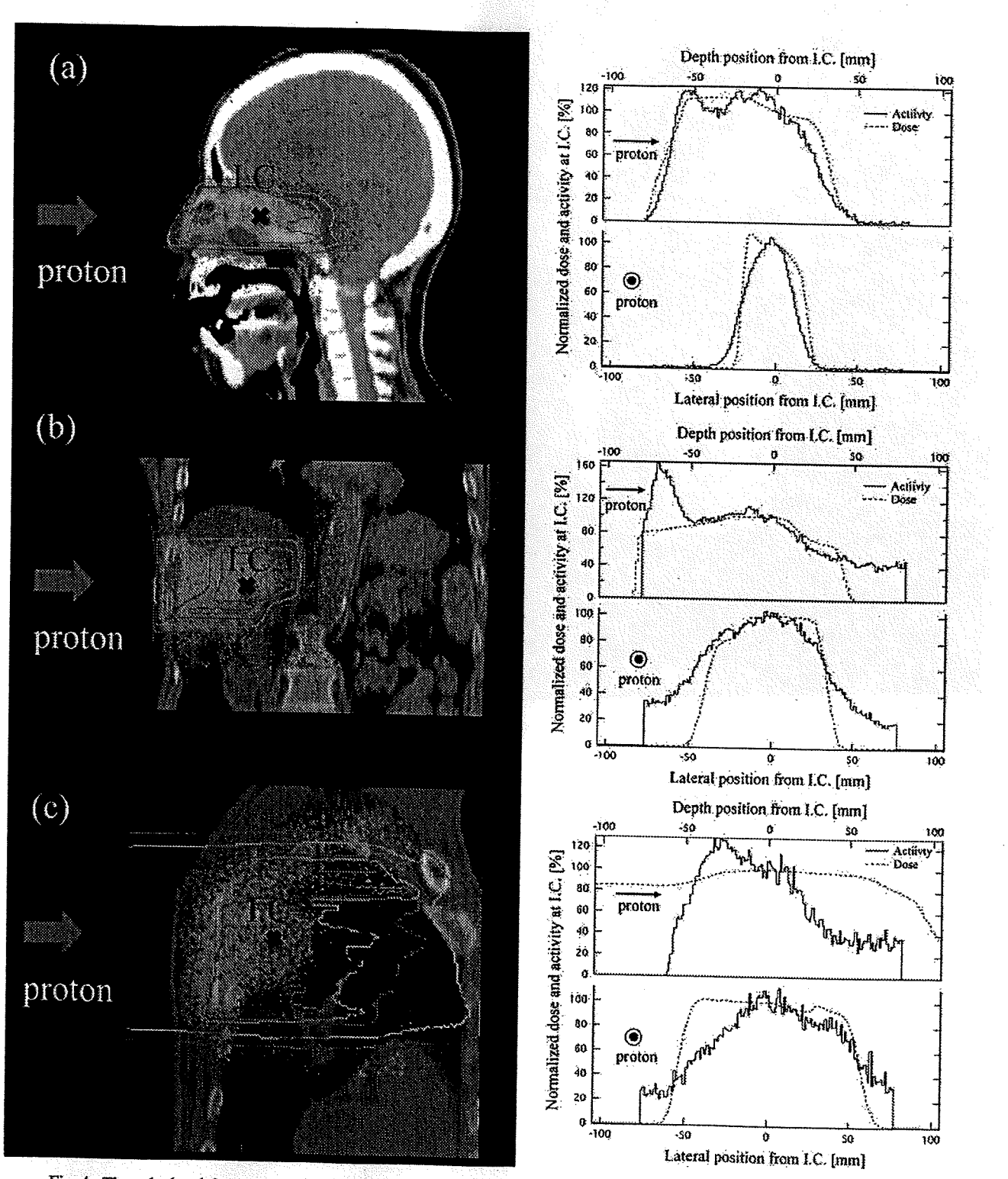

Fig. 4. The calculated dose distribution and the measured activity distribution (left figure), and corresponding lateral and depth profiles (right figure) of the irradiation fields (see Table 1) in each case involving tumors of the head and neck (a), the liver (b), the lungs (c), the prostate (d), and the brain (e), respectively. The iso-dose line of 100% is red, 80% yellowish green, 50% light blue, and 20% purple. The iso-activity wash between 30% and 100% changed from light blue to red.

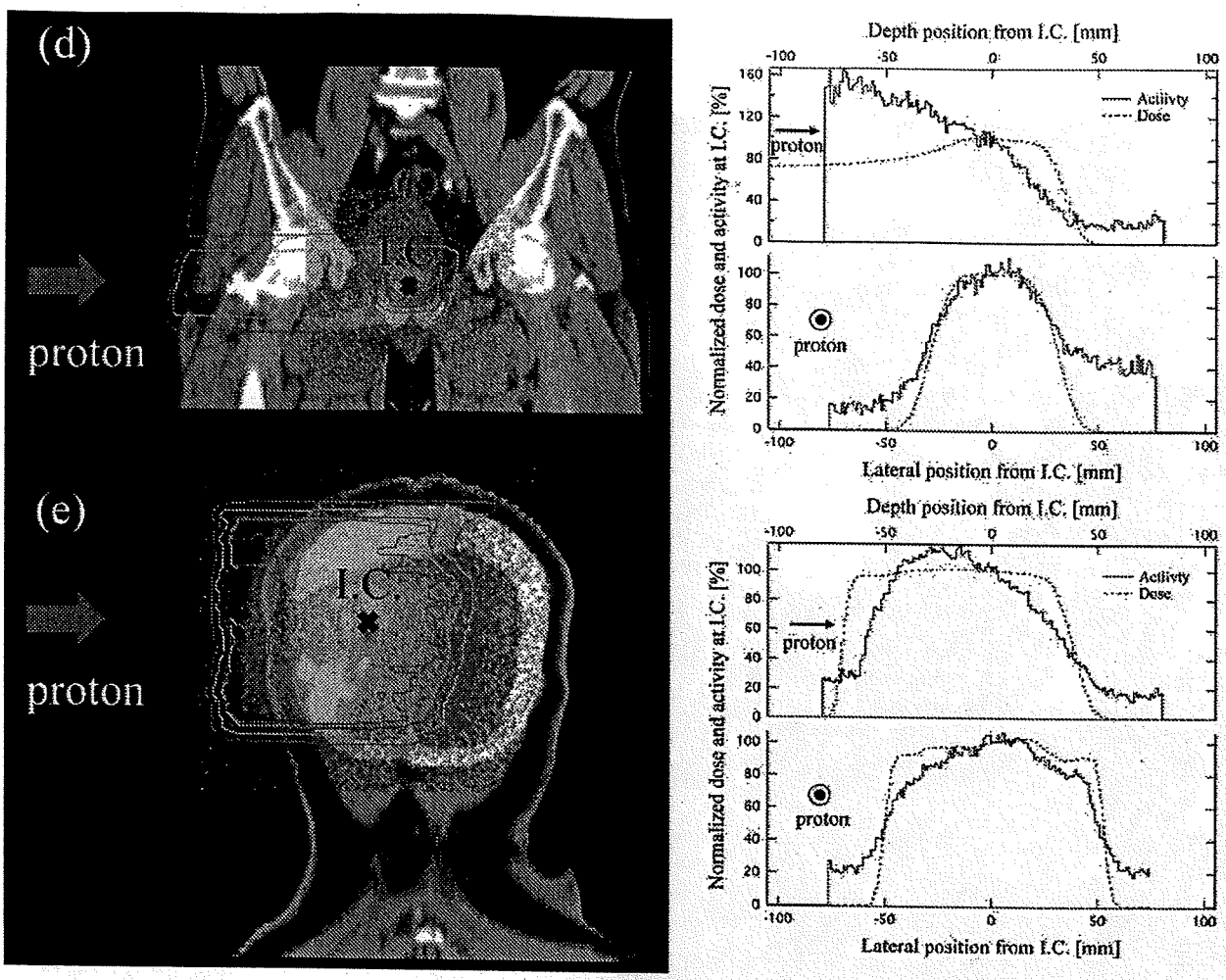

Fig. 4. *(continued)*.

of the tumor's volume was more than 100 mL. Also, in carbon therapy, similar observation of the tumor shrinkage has been reported in (7). The BOLPs-RGp indicated that the proton irradiation dose was delivered to the brain stem of organs at risk.

Washout effect of the activity in the treatment period

A histopathologic examination demonstrated that higher activity was observed in regions containing necrotic liver cells than in any other region. The upper panel of Fig. 7 shows the calculated dose distribution and the measured activity distribution on a CT image taken at the first treatment of a 3.8 GyE delivery dose. The bottom left panel of Fig. 7 shows the number of detection counts per 20 s of activity in the regions of interest of areas A and B in the liver. Hence, the region of interest of area A is the necrotic region of the tumor, and area B is the normal tumor region. Therefore, area B-A is equivalent to the area of the tumor minus the necrotic region. The observed decay curves in the region of interest of area A and B-A were fitted well enough using a double exponential equation. The two half-lives of the double exponential fitting were 31 ± 8 s and 146 ± 20 s in the area A, and 21 ± 4 s and 164 ± 11 s in the area B-A, respectively. The half-life was longest in the necrotic region of the tumor. The activity images for the 200 s measurement by the BOLPs-RGp are shown in the left of Fig. 8. The high activity

Table 1. Summary of proton beam irradiation parameters

	Treatment site	Proton energy [MeV]	SOBP [mm]	Gantry angle [deg.]	Bed angle [deg.]	Fractional dose [GyE]	Irradiation time [sec.]
(a)	Head and Neck	123	90	0	0	2.5	39
(b)	Liver	137	70	270	0	3.8	229
(c)	Lungs	145	70	160	0	2.0	38
(d)	Prostate	187	50	270	0	2.0	15
(e)	Brain	122	90	330	90	2.5	40

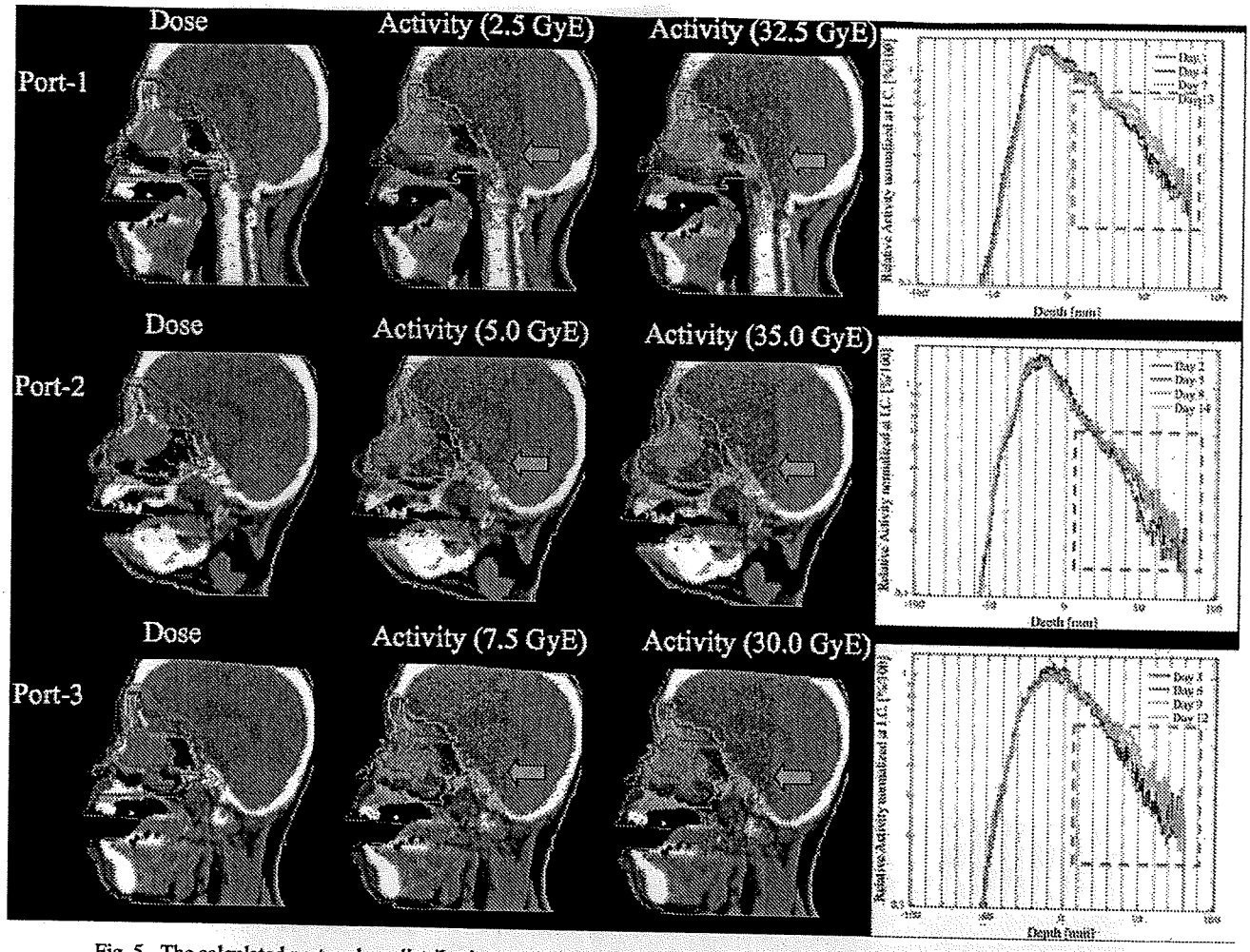

Fig. 5. The calculated proton dose distribution, measured activity distribution of a 2.5-GyE dose irradiation, and the depth profile of the measured activity normalized to the iso-center (0-mm depth) of the reference activity after a delivery dose of 2.5–35.0 GyE.

of the necrotic region decreased to same level as the normal parts of the liver in the last treatment. The ratio F of the detection activity normalized to the activity data from the first treatment for the delivery doses in the area A and the area B-A is expressed as follows:

$$F(D) = \frac{\int_0^{S_A} \left(dN(D)/dS\right) dS / \int_0^{S_A} dS}{\int_{S_A}^{S_B} \left(dN(D)/dS\right) dS / \int_{S_A}^{S_B} dS}. \quad (2)$$

Here, N is the detection number, S_A is the square of area A, and S_B is the square of area B. Ratio of the F values normalized at the value in first treatment calculated by using Eq. 2 and proton beam irradiation time per fraction dose are shown in the right of Fig. 8. The average of the irradiation time at random was 159 ± 77 s. There was no correction in the irradiation time and the decrease of the activity shown in Fig. 8. A decrease in the activity of the necrotic region was observed after the delivery dose was increased without depending on the beam irradiation time per fraction dose.

DISCUSSION

This study focused on the development of the BOLPs-RGp and its clinical use against tumors of the head and neck, liver, lungs, prostate, and brain in the proton therapy. Quick measurement of the activity generated in a patient's body after proton irradiation is feasible by using the BOLPs-RGp. The elements tracked by the activity imaging are ^{11}C (20.39 min), ^{10}C (19.26 s), ^{13}N (9.965 min), ^{15}O (122.2 s), ^{14}O (70.61 s), ^{30}P (2.498 min), and ^{38}K (7.636 min), and according to the results of a simulation by Parodi *et al.*, the "key" positron emitter nuclei are ^{11}C and ^{15}O (14). The measurement of this activity must be immediately performed after proton irradiation as the half-life of ^{15}O is about 2 min. As a result, the information for activity imaging is obtained in a short period. On the other hand, in the case of a beam OFF-LINE PET system used with a commercial based PET or PET/CT apparatus, it is very difficult to measure the activity of ^{15}O for several minutes even at the start of the activity measurement after proton irradiation. The main elements used for activity imaging are ^{15}O for measurements with